A Lightweight, Simple-structure, Low-cost and Compliant Continuously Variable Transmission Based on Twisted String Actuator

Chanchan Xu, Tong Liu, Shuai Dong, Xiaojie Wang

***Abstract*—This paper presents a novel Continuously Variable Transmission (CVT) based on a Twisted String Actuator (TSA), capable of automatically adjusting its Transmission Ratio (TR) in response to external loads. Utilizing lightweight hyperelastic slender rods, the CVT achieves a simple, compact, and cost-effective design. By manipulating the distance between two twisted strings through rod deformation, the TR continuously adapts to varying load conditions. Mathematical models of the TSA-based CVT system are derived and experimentally validated, demonstrating a 2.1-fold TR variation from 0.1 kg to 1.5 kg loads. Application in an anthropomorphic robot finger showcases a 6.2-fold TR change between unloaded and loaded states. Our CVT offers unparalleled advantages in weight, cost, simplicity, compliance, and continuous TR adjustability, making it highly suitable for robotic systems.**

***Index Terms*—Continuously variable transmission, twisted string actuator, anthropomorphic robot finger**

I. Introduction

The development of CVT mechanisms is essential in enabling robotic systems to achieve both high-speed motion and substantial load capacity, thereby enhancing actuator efficiency [1]. Various CVT devices have been devised, encompassing wheel-type CVT, belt CVT, chain CVT, toroidal CVT, spherical CVT, among others [2]–[5]. Each variant offers distinct approaches to achieving continuous variation in transmission ratios, each with its own set of advantages and constraints.

TSA represents a noteworthy soft actuator type, comprising one or more strings, an electric motor, and a load. They adeptly convert rotational motion from the motor into linear motion by winding the string(s). Owing to their straightforward design, high TR, substantial output force, and compliance, TSA has found application in a myriad of fields, including robotic hands, rehabilitation robots, and soft robots [6], [7]. However, optimizing TSA performance necessitates integration with a CVT mechanism to tailor its TR in accordance with operational loads, typically achieved through modifications in string radius, string distance, or input torque.

Shin et al. [8] pioneered a passive dual-mode transmission mechanism rooted in TSA principles. In force mode, strings intertwine, while in speed mode, they rapidly coil around a thick shaft, effectively augmenting the string's radius. Despite offering a wide transmission ratio range, mode switching is beset by uncertainty owing to time-varying friction, leading to significant energy loss. To mitigate this challenge, the team proposed an active dual-mode VT by incorporating a secondary motor [9]. However, this solution comes at the expense of compliance and introduces complexity. Furthermore, the dual-mode VT merely offers discrete TR levels, lacking continuous adjustment. Lu et al. [10] realized continuous automatic TR adjustment predicated on external load variations by compressing springs to varying extents, thereby inducing the string to wind around a shaft of variable radius. Nevertheless, their mechanism, characterized by a complex architecture and friction-induced energy losses, presents notable drawbacks. Additionally, Park's team [11] devised an elastomeric CVT-based TSA for automatic TR adjustment based on load size. Unlike Lu et al., they achieved continuous TR adjustment by modulating the input torque of the string according to the external load, accomplished by compressing the elastomer linked to the string's end. Nonetheless, the torque transmission pathway, from the motor through spur gears to a rigid lateral disc, reliant on friction between the disc and elastomer, harbors the risk of energy dissipation, silicon abrasion, and slippage. Consequently, its viability for large robot devices is compromised by the inherent friction limitations of the elastomer. Similarly, Shin et al. [12] engineered a CVT-based TSA by manipulating the input torque of the string in response to the external load. While their CVT delivers a twofold increase in TR compared to Park's team, its highly intricate and bulky nature renders it unsuitable for lightweight robots.

In the pursuit of a lightweight and simplistic CVT system, Ryu's team [13] introduced a passive TSA-based CVT that adjusts TR by varying the distance between two strings using springs, contingent on external load fluctuations. Despite its relatively lightweight and straightforward design, the spring-based CVT still suffers from enlarged dimensions, rendering it less conducive for small robots. Moreover, to achieve continuous active TR adjustment, the team devised an active-type TSA-based CVT employing planetary gears [14]. However, the incorporation of planetary gears and a secondary motor

Corresponding author: Shuai Dong (e-mail: shuaizhi@ustc.edu.cn), Xiaojie Wang(e-mail: xjwang@iamt.ac.cn)

Chanchan Xu and Tong Liu are with the Institute of Intelligent Machines, Hefei Institutes of Physical Science, Chinese Academy of Sciences, Hefei 230031, China, and also with the University of Science and Technology of China, Hefei 230026, China (e-mail: xuchan@mail.ustc.edu.cn; lt1997@mail.ustc.edu.cn).

Shuai Dong is with the Department of Precision Machinery and Precision Instrumentation, University of Science and Technology of China, Hefei 230026, China (e-mail: shuaizhi@ustc.edu.cn).

Xiaojie Wang is with the Institute of Intelligent Machines, Hefei Institutes of Physical Science, Chinese Academy of Sciences, Hefei 230031, China (e-mail: xjwang@iamt.ac.cn).

TABLE I
THE PERFORMANCE COMPARISON WITH OTHER EXISTING TSA-BASED VTS

TSA-based VT types		Weight of VT	Size of VT	Complexity of VT'structure	Cost of VT	Compliant ?	Continuous ?	Range of TR adjustment
Our CVT		0.22 g	1 mm*1 mm*30 mm	Very simple	$0.041	Yes	Yes	2.1 times
Dual-mode	Passive [8]	>10 g	-	Moderate	>$1	No	No	-
	Active [9]	>29.6 g	69.2 mm*19.5 mm*15 mm	Complex	>$214	No	No	6.95 times
PVT [13]		80 g	>15 mm*40 mm*80 mm	Simple	>$1	Yes	Yes	<2 times
ElaCVT [11]		12 g	24 mm*24 mm*42 mm	Complex	>$10	Yes	Yes	2.31 times
Pat-CVT [12]		1.4 kg	85 mm*120.5 mm*115 mm	Very complex	>$10	Yes	Yes	4.6 times
Active CVT [14]		133.6 g	45 mm*45 mm*129 mm	Complex	>$232	No	Yes	1.78 times
LAHM [10]		>10 g	>14 mm*14 mm*67 mm	Complex	>$1	Yes	Yes	2.1 times

amplifies system weight, size, and cost, at the expense of compliance. Notwithstanding the plethora of TSA-based VTs developed, there persists a demand for a VT that is exceedingly lightweight, mechanically simple, compact, cost-effective, intrinsically compliant, continuous, and suitable for both small and large-scale robotic applications.

To address this imperative, we present a novel TSA-based CVT capable of continuously adjusting TR by modifying the distance between two twisted strings in response to external load variations. Our CVT comprises solely a pair of extremely lightweight hyperelastic slender rods, measuring a mere 1 mm * 1 mm * 30 mm, weighing 0.22 g, and costing only $0.041. Its TR undergoes a 2.1-fold variation as the load transitions from 0.1 kg to 1.5 kg. Comparative analysis against existing TSA-based VTs in Table I underscores our proposed TSA-based CVT as the lightest, simplest in structure, and most cost-effective option. Furthermore, it boasts compliance and continuity, rendering it suitable for a plethora of robotic tasks across various scales.

The subsequent sections are structured as follows: Section II elucidates the proposed design concept and operational mechanism of the TSA-based CVT. Section III furnishes a theoretical analysis of the TSA-based CVT system. In Section IV, we delineate an experimental setup aimed at validating the efficacy of the proposed mechanism and the established theoretical model. Finally, in Section V, we demonstrate the application of the proposed TSA-based CVT to an anthropomorphic robot finger.

II. CONCEPT OF THE PROPOSED CVT

Actuators employed in robotic systems are expected to exhibit a smaller TR for swift motion when operating without a load, and a larger TR for delivering substantial supporting force at lower speeds when subjected to a load. To achieve this objective, we propose a CVT based on TSA that automatically adjusts its TR according to the load weight. The structure and mechanism of the proposed TSA-based CVT are illustrated in Figure 1. The proposed TSA-based CVT consists of a

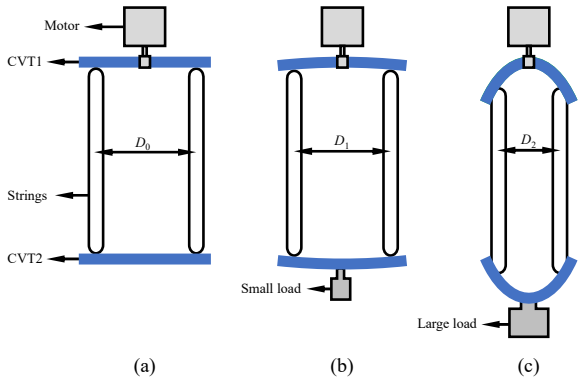

Fig. 1. The TSA-based CVT mechanism. (a) The state without load. (b) The state with a small load. (c) The state with a large load.

pair of CVTs (CVT1 and CVT2) integrated within the TSA framework. CVT1 is linked to the motor's output shaft, while CVT2 is connected to the load. Both CVT1 and CVT2 comprise hyperelastic rods, interconnected by two strings. When CVT2 bears a lighter load, it undergoes minimal deformation. The distance between the strings is large, allowing rapid contraction, resulting in a small TR. Conversely, under heavier loads, CVT2 undergoes bending deformation, reducing the distance between the strings and slowing down the contraction speed, thereby increasing the TR and enhancing load capacity. As the load magnitude increases, the bending deformation of CVT2 intensifies, resulting in a smaller string distance, further increasing the TR and enhancing load capacity.

III. THEORETICAL ANALYSIS FOR THE PROPOSED CVT

In this section, we develop a mathematical model for the proposed TSA-based CVT which describes the relationship between input and output displacements, thereby characterizing the TR of the entire system. Additionally, we verify the effectiveness of the proposed TSA-based CVT through theoretical computational results.

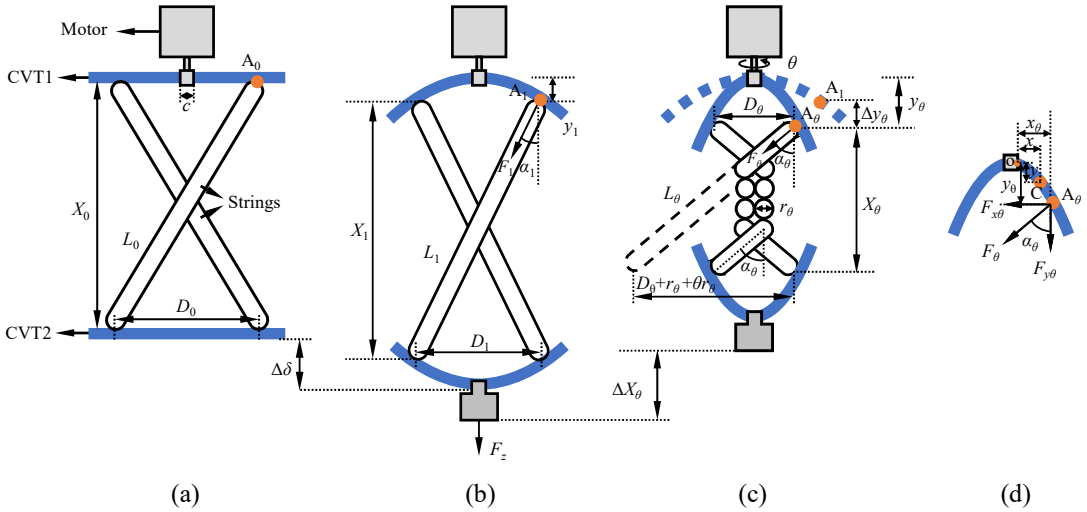

Fig. 2. The proposed TSA-based CVT with pre-twisted half a turn for initial state without load (a) and with load (b). (c) The state with load after the motor makes a certain number of turns θ. (d) Force analysis for CVT1.

A. Mathematical model

The proposed TSA-based CVT is the combination of TSA and CVT. Notably, the conventional mathematical model for TSA initially assumes the strings to be rigid, overlooking the fact that the strings possess stretchable properties. While the conventional model simplifies the modeling process, it compromises the model's precision. Consequently, in our modeling approach, we consider the strings to be stretchable, with an associated stiffness coefficient denoted as K. Furthermore, we consider the CVT as a hyperelastic material, assuming its deformation to be within its elastic range and characterized by a constant elastic modulus E. To avoid an abrupt contraction of strings leading to an uncomfortable linear motion of load, the string is pre-twisted half a turn, as illustrated in Figure 2(a). Once this pre-twisting is applied, we can calculate the initial distance, denoted as X_0, which represents the vertical distance between the connection points of the two CVTs and the strings on the same side, using the following formula:

$$X_0 = \sqrt{L_0^2 - D_0^2} \tag{1}$$

where, L_0 represents the initial length of the string without load force, and D_0 is the initial distance between the ends of the CVT and the string connection without load force. When a workload is attached to CVT2, as depicted in Figure 2(b), the strings experience tension, causing them to stretch from L_0 to L_1. This simultaneously induces bending deformations in CVT1 and CVT2, leading to a reduction in the distance between the ends of the CVT and the string connection from D_0 to D_1 and an increase in the vertical distance between the connection points of the two CVTs and the string on the same side from X_0 to X_1.

As the motor rotates by an angle θ, the strings undergo a corresponding twisting motion, forming a cylindrical shape with a radius of r_θ in their midsection, as depicted in Figure 2(c). This results in an increase in the tension experienced by the strings, causing their axial length to transition from L_1 to L_θ. Concurrently, CVT1 and CVT2 undergo further bending, resulting in a transition of the distance between the ends of the CVT and the string connection from D_1 to D_θ. Ultimately, this leads to a decrease in the vertical distance between the connection points of the two CVTs and the strings on the same side to X_θ, thereby inducing a linear motion of the load denoted by ΔX_θ. L_θ can be calculated by

$$L_\theta = L_0 + \frac{F_\theta}{K} \tag{2}$$

$$F_\theta = \frac{F_z}{2\cos\alpha_\theta} \tag{3}$$

where, F_θ represents the axial tension of the string when it is twisted by an angle θ, and F_z represents the load force. Additionally, α_θ is the angle between the string and the motor axis direction when it is twisted by an angle θ. We assume that the helix angle of the formed cylinder is evenly distributed across the twists of the strings, thus, the helix angle equals the angle between the string and the motor axis direction, α_θ. Now suppose one of the strings is unwound geometry of a cylinder, as shown in Figure 2(c), so

$$\cos\alpha_\theta = \frac{X_\theta}{\sqrt{X_\theta^2 + (D_\theta + r_\theta + \theta r_\theta)^2}} \tag{4}$$

$$X_\theta = L_\theta \cos\alpha_\theta = L_0 \cos\alpha_\theta + \frac{F_z}{2K} \tag{5}$$

The assumption of variable string radius was proved in [15]. However, given the elasticity of the strings, which experience deformation under tension, we've taken into account the impact of the applied load force on the radius. As a result, we approximate the radius r_θ of the cylindrical shape formed by the middle section of the strings using the following relationship:

$$r_\theta = \left(\frac{1}{k_1 F_z} + k_2 + k_3\sqrt{X_0/X_\theta}\right) r_0 \tag{6}$$

where k_1, k_2, and k_3 represent approximation coefficients that depend on the structure and mechanical properties of the

strings, and r_0 stands for the diameter of the string when they are in an unloaded state.

To determine D_θ, we conduct a force analysis on CVT1, as depicted in Figure 2(d). CVT1 is fixed to the motor's output shaft via a fixture of width c. The two ends of CVT1 experience bending deformation due to the tension in the two strings. Here, CVT is considered as a slender rod with a diameter d, which allows for the force and deformation characteristics of CVT1 to be likened to those of two symmetric cantilever beams, each subjected to concentrated loads at their endpoints. Therefore, we opt to analyze the force and deformation on the right half of CVT1. Selecting the center point of the right end face of the fixture as the coordinate origin O, and assuming that the entire assembly reaches equilibrium after the strings have twisted through an angle θ. We define the horizontal distance from any point C on the right half of CVT1 to O as x and the vertical distance to O as y. The resulting deformation of the bending curve satisfies the following flexural curve differential equation:

$$\frac{d^2y/d^2x}{(1+(dy/dx)^2)^{3/2}} = \frac{M}{EI} \tag{7}$$

where M represents the moment experienced at point C and I is the moment of inertia of the cross-section, where $I = \frac{\pi d^4}{64}$.

Point A_θ is the connection point between CVT1's right end and the string, bearing a concentrated load F_θ applied by the string. Let x_θ denote the horizontal distance from point A_θ to the origin O, and y_θ represent the vertical distance from point A_θ to the origin O. Thus, the coordinates of point A_θ can be expressed as $(x_\theta,\ y_\theta)$. By breaking down the tension F_θ at point A_θ into horizontal force $F_{x\theta}$ and vertical force $F_{x\theta}$, we have:

$$\begin{cases} F_{y\theta} = F_z/2 \\ F_{x\theta} = F_z \tan\alpha_\theta/2 \end{cases} \tag{8}$$

Consequently, the moment M experienced at point C can be calculated as follows:

$$M = F_{y\theta}\left(x_\theta - x\right) + F_{x\theta}\left(y_\theta - y\right) \tag{9}$$

Assuming that the shape of the right half of CVT1 forms a quadratic curve after deformation, the relationship between y and x is as follows:

$$y = ax^2 \tag{10}$$

where a is the coefficient of the quadratic curve. Substituting (8), (9) and (10) into (7), we obtain:

$$\frac{2aEI}{(1+4a^2x^2)^{3/2}} = F_{y\theta}\left(x_\theta - x\right) + F_{x\theta}\left(ax_\theta^2 - ax^2\right) \tag{11}$$

Assuming that the length of the right half of CVT1 remains unchanged before and after deformation, we have:

$$2\int_0^{x_\theta} \sqrt{1+(2ax)^2}dx + c = D_0 \tag{12}$$

Finally, the load contraction of proposed TSA-based CVT, represented by ΔX_θ, can be expressed as:

$$\Delta X_\theta = X_1 - X_\theta - 2\Delta y_\theta = X_1 - X_\theta - 2\left(y_\theta - y_1\right) \tag{13}$$

where y_1 represents the vertical distance between point A_θ and point O when the strings with load are twisted by half a rotation, and Δy_θ is the distance by which point A_θ moves downward when the strings with load twist from half a rotation to θ. By solving equations (5), (11), and (12) together, we can determine the values of X_θ and y_θ. Setting $\theta = \pi$ in these equations allows us to solve for X_1 and y_1. Further, we can resolve ΔX_θ. Thus, the TR of the proposed TSA-based CVT is expressed as follows:

$$TR = \frac{1}{\partial\left(\Delta X_\theta\right)/\partial\theta} \tag{14}$$

B. Theoretical results

TABLE II
THE PARAMETERS USED IN THEORETICAL MODEL

L_0 (m)	D_0 (m)	c (m)	r_0 (m)	d (m)	K (N/m)	E (GPa)	k_1 (1/N)	k_2	k_3
0.097	0.032	0.006	0.0015	0.001	1370	37	7.1	0.22	0.224

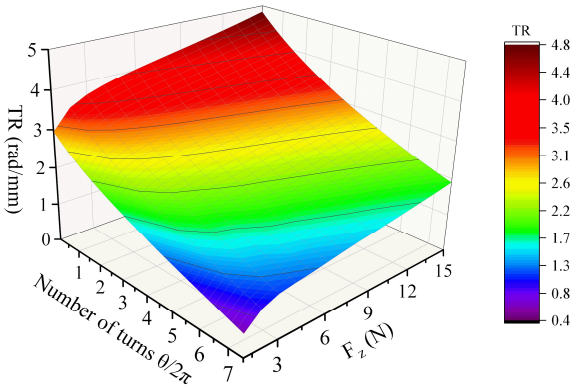

Fig. 3. Theoretical TR of the proposed TSA-based CVT varied with the number of turns of the motor and load F_z.

We validate the effectiveness of the proposed TSA-based CVT through theoretical analysis. Theoretical computational results depicting how the TR varies with the number of motor turns under various loads F_z are presented in Figure 3. The parameters utilized in the theoretical model are outlined in Table II. It is observed that as the number of motor turns increases, the TR gradually decreases, consistent with the findings of Ryu's team [13]. Additionally, under the same number of motor turns, the TR increases with increasing workload, particularly noticeable with lower loads. Under the initial condition of half a turn pre-twist, the TR escalates from 2.95 rad/mm to 4.83 rad/mm with the load ascending from 1 N to 15 N, marking a 1.6-fold increase. Moreover, with a pre-twist of 7.5 turns from the initial state, the TR surges from 0.59 rad/mm to 1.89 rad/mm, demonstrating a 3.2-fold rise under the corresponding load conditions. For lighter loads, the TSA-based CVT demonstrates lower TR, resulting in faster contraction speed. Conversely, for heavier loads, the TSA-based CVT shows higher TR, leading to slower contraction

speed but enhanced load capacity. Thus, the effectiveness of the designed TSA-based CVT is theoretically confirmed.

IV. Performance Evaluation for Proposed CVT

In this section, we developed an experimental setup to test the performance of the designed TSA-based CVT and experimentally confrm the effectiveness of the proposed TSA-based CVT mechanism. Additionally, we validated the previously established theoretical model by comparing the experimental and theoretical values of TSA's contraction.

A. Experimental setup

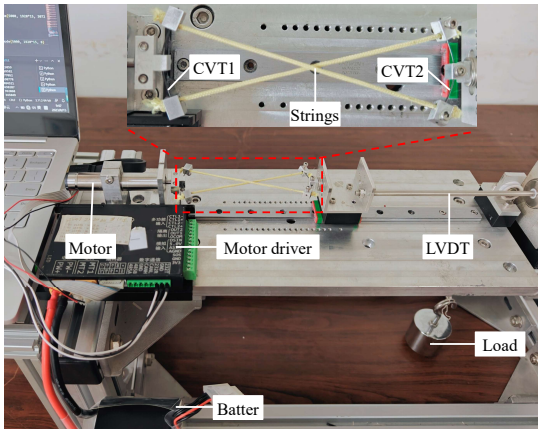

Fig. 4. The test platform for property of TSA-based CVT.

Figure 4 showcases the experimental setup utilized to assess the TR change capability of the TSA-based CVT under varying loads. The key components of the setup included a direct current (DC) motor (Maxon DCX16L) controlled by an RMDS-405 motor driver, a pair of CVTs (CVT1 and CVT2), two strings, a load, a linear guideway (Hiwin, MG), and a linear variable differential transformer (LVDT, W-DC) with a stroke of 20 cm. The DC motor was horizontally mounted on a frame and operated via the RMDS-405 motor driver. The load and LVDT were securely affixed to the linear guide. We conducted experiments using parameters consistent with those listed in Table II. For the CVTs, two Ni-Ti memory alloy rod with a diameter of 1 mm, a length of 32 mm, and an elastic modulus of 37 Gpa, exhibiting superelastic characteristics, was utilized. CVT1 was connected to the output shaft of the motor using a 6 mm wide fixture, while CVT2, also with a 6 mm wide fixture, was positioned parallel to CVT1 on the linear guide. Two braided ultrahigh molecular weight polyethylene (UHMWPE) fiber strings, each with a diameter of 1.5 mm, an initial length of 97 mm without external loads and the stiffness coefficient of 1370 N/m, were employed for the TSA. These strings were connected at either end of CVT1 and CVT2 in parallel to the motor's axis. To prevent sudden load movement, the strings were pre-twisted half a turn. Subsequently, the motor drove CVT1 to continuously rotate with constant speed of 12.5 rpm/min for 7.5 turns under different loads.

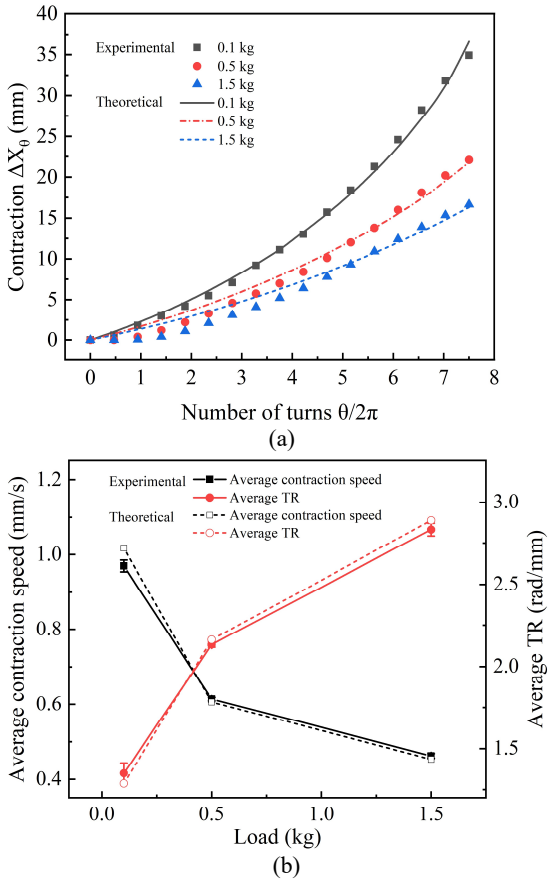

Fig. 5. The performance test results of the proposed TSA-based CVT. (a) The experimental and theoretical load contractions for the proposed TSA-based CVT varied with the number of turns of the motor, maintaining a constant output speed of 12.5 rpm/min, while carrying workloads of 0.1 kg, 0.5 kg, and 1.5 kg, respectively. (b) The experimental and theoretical average contraction speed of load and average TR varied with the load, maintaining a constant motor output speed of 12.5 rpm/min.

B. Results

The performance test results of the proposed TSA-based CVT are illustrated in Figure 5. In Figure 5(a), the experimental and theoretical load contractions for the proposed TSA-based CVT are depicted, showcasing variations with the number of motor turns across different loads. It is observed that as the number of motor turns increases, the load contraction gradually increase. Under the same number of motor turns, load contraction decrease with increasing workload, particularly evident with a higher number of turns. The TSA-based CVT exhibits maximum contractions of 34.9 mm, 22.1 mm, and 16.64 mm when carrying workloads of 0.1 kg, 0.5 kg, and 1.5 kg, respectively. Comparing load contraction, there is a 36.7 % decrease from 0.1 kg to 0.5 kg and a 24.7 % decrease from 0.5 kg to 1.5 kg, and a 52.3 % decrease from 0.1 kg to 1.5 kg. The TSA-based CVT exhibits greater sensitivity to load variations from 0.1 kg to 0.5 kg compared to from 0.5 kg to 1.5 kg.

Additionally, Figure 5(b) illustrates experimental and theoretical data concerning the average contraction speed of the load and the average TR as they vary with the load. The results show that the theoretical average contraction speed

of the load and average TR closely aligns with experimental results. Moreover, there is a decreasing trend in the average contraction speed of the load with increasing workload, while the average TR of the TSA-based CVT exhibits a corresponding increase with workload. Under loads of 0.1 kg, 0.5 kg, and 1.5 kg, the TSA-based CVT demonstrates experimental average contraction speeds of 0.97 mm/s, 0.61 mm/s, and 0.46 mm/s, respectively. Correspondingly, the experimental average TR varies at 1.35 rad/mm, 2.13 rad/mm, and 2.83 rad/mm for these respective loads. Notably, under a 1.5 kg load, the experimental contraction speed diminishes to 47.4 % of that observed under a 0.1 kg load, while the average TR increases to 2.1 times. When the load is lighter, the TSA-based CVT demonstrates reduced TR, facilitating quicker contraction rates. Conversely, under heavier loads, the TSA-based CVT displays elevated TR, resulting in slower contraction rates but increased load capacity.

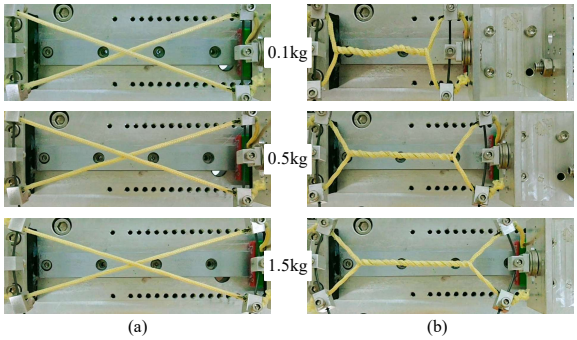

Fig. 6. Snapshot of TSA-based CVT carrying workloads of 0.1 kg, 0.5 kg, and 1.5 kg. (a) In the initial state for pre-twisted half a turn with load. (b) After being twisted 7.5 turns from the initial state.

This phenomenon is demonstrated in Figure 6, which presents snapshots of the TSA-based CVT carrying loads of 1 kg, 0.5 kg, and 1.5 kg in the initial state with half a turn of pre-twist with the load (Figure 6(a)), and subsequent to being twisted 7.5 turns from the initial state (Figure 6(b)). In Figure 6(a), it is observed that when the load is 0.1 kg, the CVT undergoes minimal deformation in the initial state, with the distance between the ends of the CVT and the string connection (D) being 32 mm. With increasing turns, D remains almost unchanged, indicating that the CVT effectively operates as if under a fixed offset of 32 mm, resulting in relatively faster contraction speeds. When the load is 0.5 kg, there is a slight change in the CVT from 32 mm to 31 mm in the initial state, indicating a smaller change compared to the 0.1 kg load. However, as the turns increase, the tension on the string gradually increases, causing the CVT to bend and D to decrease while increasing the downward displacement (Δy_θ) of the ends of the CVT and the string connection. D decreases to 28.9 mm after 7.5 motor turns. The comprehensive effect of load contraction, resulting from both the contraction of the string ($X_1 - X_\theta$) and the downward displacement of the CVT (Δy_θ) due to bending, is described by Equation 13. A larger ($X_1 - X_\theta$) leads to faster load contraction, while a larger Δy_θ results in slower load contraction. As D decreases with increasing turn, accompanied by an increase in Δy_θ, there is a dual reduction in the load contraction speed, which becomes more pronounced with higher load. When the load increases to 1.5 kg, the CVT exhibits significant initial bending, reducing D to 29.2 mm, which further decreases to 25.9 mm after 7.5 motor turns, resulting in even slower load contraction. Therefore, the experiments demonstrate that the proposed TSA-based CVT can automatically adjust TR according to external load variations to meet the system's requirements.

Moreover, from Figure 6(a), it is evident that our established theoretical model aligns well with experimental results. While the theoretical model almost coincides with experimental data for a 0.1 kg load, there are slight deviations for 0.5 kg and 1.5 kg loads during the initial twisting stage, likely due to gaps within the braided string and the nonlinearity of the elastic modulus of the superelastic materials used in the CVT under higher load. Overall, our established model effectively predicts the load contraction of TSA-based CVT. This model serves as a valuable theoretical tool for analyzing and optimizing the performance of TSA-based CVT.

V. Application for an Anthropomorphic Robot Finger

In this section, we apply the proposed TSA-based CVT to an anthropomorphic robot finger and test its adaptability to the external load, further validating the practicality of the proposed TSA-based CVT.

A. Design and Working mechanism

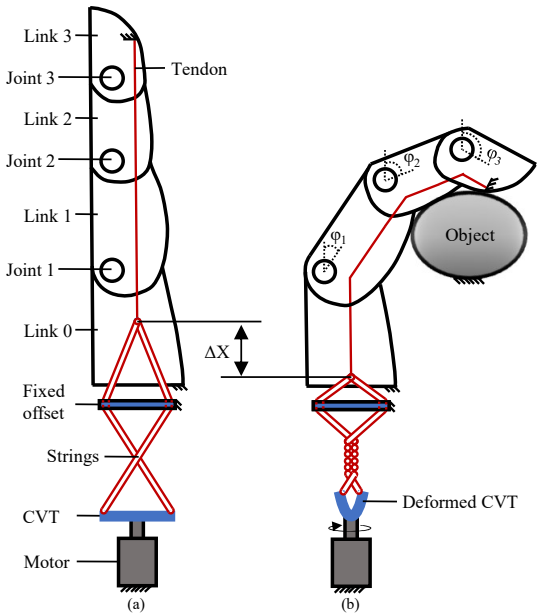

Fig. 7. The design principle of the proposed anthropomorphic robot finger with proposed TSA-based CVT. (a) The initial state for pre-twisted half a turn without load. (b) The state after grasping the object.

Figure 7 illustrates the design principle of the proposed anthropomorphic robot finger with proposed TSA-based CVT. The anthropomorphic robot finger comprises a 3D-printed finger including 4 links and 3 rotating joints, and TSA-based CVT system. Link 0 is fixed, while links 1, 2, and 3 can

rotate around joints 1, 2, and 3 respectively, with all three joints equipped with elastic rings to provide resilience. To prevent rotation at the output end of the CVT system, only an superelastic rod is employed near the motor end, while a fixed offset is utilized near the load end. The output end of the CVT system is connected to the fingertip via a tendon. The finger's flexion is driven by the contraction force of the strings when the motor twists them, while extension is achieved through the rebound force of the elastic rings at joints when the strings are untwisted.

The mechanism of the anthropomorphic robot hand with proposed TSA-based CVT operates as follows: when the finger is not in contact with a load, the contraction force of the strings is minimal, and the CVT remains nearly unchanged. The distance between the strings is large, allowing rapid contraction, resulting in a small TR, thereby enabling the finger to quickly make contact with an object. Once the finger contacts an object, the contraction force of the strings increases, causing the CVT to bend and deform, reducing the distance between the strings and slowing down the speed of contraction. Consequently, the TR of the entire system increases, resulting in slower grasping speed but enhanced gripping capability. As the load increases, the degree of bending and deformation of the CVT becomes more pronounced, further reducing the distance between the strings and increasing the overall TR. Therefore, the anthropomorphic robot finger can adjust its TR according to the operational load conditions.

B. Performance evaluation

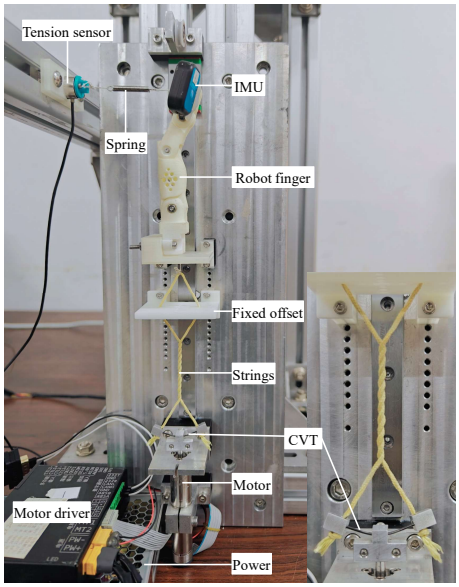

Fig. 8. Experimental setup to evaluate the proposed anthropomorphic robot hand.

To assess the TR change capability to variable load of the proposed anthropomorphic robot finger, we designed an experimental setup as depicted in Figure 8. The motors (Maxon DCX16L) equipped with encoders (Maxon ENX16) were controlled using an RMDS-405 driver. The distance between the strings with fixed offset is 30 mm. An superelastic Ni-

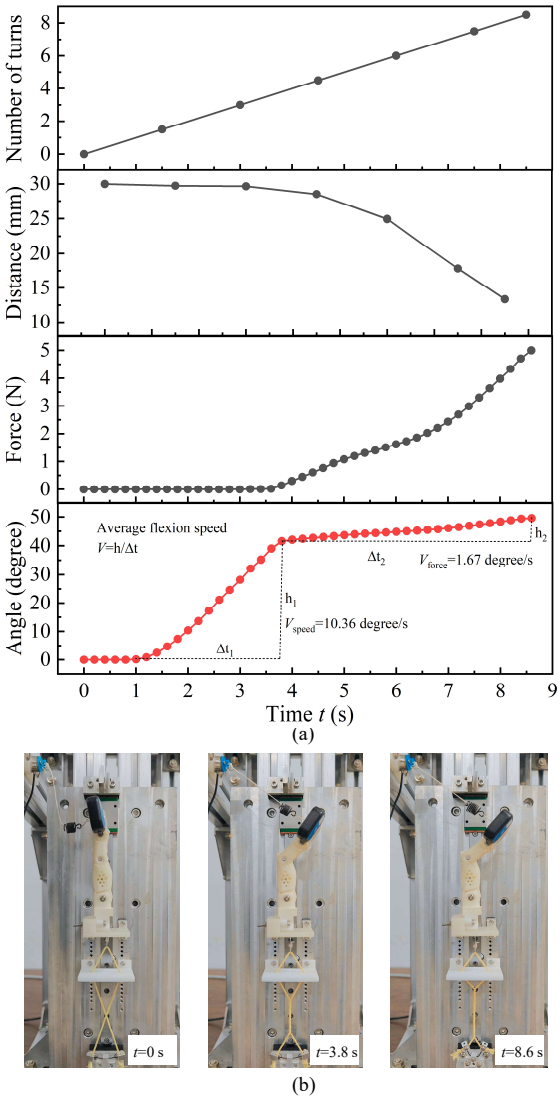

Fig. 9. The results of the adaptability assessment of the proposed anthropomorphic robot hand. (a) illustrates the number of turns of the motor, the distance between the ends of the CVT and the string connection, the fingertip force provided by the spring, and the flexion angle of rotation of link 2 of the finger around joint 2 over time with a constant motor output speed of 60 rpm/min, respectively. (b) displays the motion states of the proposed anthropomorphic robot hand at time intervals of 0 s, 3.8 s, and 8.6 s.

Ti memory alloy rod with an initial length of 30 mm and a diameter of 1 mm was employed for CVT. The distance between the fixed offset and CVT is 86 mm. The string diameter is 1.5 mm. Given the varied motion trajectories inherent to underactuated robot fingers and the experimental objective of evaluating their capability to adapt to variable loads, joints 1 and 3 were immobilized, allowing only joint 2 to rotate freely. Consequently, an angle sensor (Inertial Measurement Units, IMUs) was affixed to link 3 to monitor the real-time flexion angle of link 2 around joint 2. A spring, connected at one end to the fingertip and at the other end to a tension sensor (SBT674 with a force of 50 N) secured on the frame, was utilized to provide the loading force. To prevent sudden finger movements, the string is pre-twisted half a turn. Subsequently, the motor drives the CVT to continuously

rotate with constant speed of 60 rpm/min for 8.5 turns. This causes link 2 to gradually rotate around joint 2 from a vertical position, gradually stretching the spring from its relaxed state. Both the IMU and tension sensor concurrently recorded data throughout the entire process.

The findings, presented in Figure 9, encompass various facets of the experiment. Figure 9(a), from top to bottom, shows the number of motor turns, the distance between the ends of the CVT and the string connection, the fingertip force provided by the spring, and the flexion angle of rotation of link 2 of the finger around joint 2 over time, respectively. Figure 9(b) showcases the sequential motion states of the proposed anthropomorphic robot hand at time intervals of 0 s, 3.8 s, and 8.6 s (further details in video-1).

It's evident that before t = 3.8 s, the spring is relaxed, providing zero force to the fingertip, and the distance between the ends of the CVT and the string connection remains almost constant. The average flexion speed of link 2 rotation around joint 2 is 10.36 degrees/s, except for the negligible motion because the initial twisting of the string doesn't significantly affect the movement of link 2. After $t > 3.8$ s, the spring gradually stretches, and the fingertip force increases from 0 N to 5 N. The distance between the ends of the CVT and the string connection is reduced to 12.4 mm, and the average flexion speed of the finger decreases to 1.67 degrees/s, indicating a notable 6.2-fold TR alteration between unloaded and loaded conditions. Additionally, from Figure 9(b), it's apparent that before the stretching of the spring, the distance between the ends of the CVT and the string connection remains nearly constant. However, after the stretching of the spring, this distance noticeably decreases. The finger's movement speed is significantly faster before the spring stretching compared to after. Therefore, the proposed anthropomorphic robot hand demonstrates the TR change capability to adapt to variable loads. It also exhibits a considerable adjustment range and can withstand at least 5 N of fingertip force. This underscores the practicality of the proposed TSA-based CVT concept.

VI. Conclusion and Future Work

In conclusion, this paper has introduced a novel CVT mechanism based on a TSA, offering automatic adjustment of TR in response to varying external loads. Through the utilization of lightweight hyperelastic slender rods, we have achieved a remarkably simple, compact, and cost-effective design. Our experimental results have validated the efficacy of the proposed TSA-based CVT, demonstrating a notable 2.1-fold TR variation across load conditions ranging from 0.1 kg to 1.5 kg. Notably, the hyperelastic rods utilized in our CVT are exceptionally lightweight and cost-efficient, with dimensions of just 1 mm * 1 mm * 30 mm, weighing 0.22 g, and costing only \$0.041. Application in an anthropomorphic robot finger has further underscored the adaptability and practicality of our CVT, revealing a significant 6.2-fold TR change between unloaded and loaded states.

This research represents a significant advancement in the field of robotic transmission systems, offering unparalleled benefits in terms of weight, cost-effectiveness, simplicity, compliance, and continuous TR adjustability. The proposed TSA-based CVT holds great promise for a wide range of robotic applications, from small-scale robots to complex anthropomorphic robotic hands. Future work will focus on refining theoretical models to account for nonlinear material characteristics and expanding the application of our TSA-based CVT to entire anthropomorphic robotic hand

VII. Acknowledgment

This work is partially supported by the Anhui Provincial Key Research and Development Program No. 2022f04020008 and National Natural Science Foundation of China No. 62301522.

References

[1] H. Yamada, "A radial crank-type continuously variable transmission driven by two ball screws," in *2012 IEEE International Conference on Robotics and Automation*. IEEE, 2012, Conference Proceedings, pp. 1982–1987.

[2] X. Chen, P. Hang, W. Wang, and Y. Li, "Design and analysis of a novel wheel type continuously variable transmission," *Mechanism and Machine Theory*, vol. 107, pp. 13–26, 2017.

[3] N. Srivastava and I. Haque, "A review on belt and chain continuously variable transmissions (cvt): Dynamics and control," *Mechanism and Machine Theory*, vol. 44, no. 1, pp. 19–41, 2009.

[4] F. Verbelen, S. Derammelaere, P. Sergeant, and K. Stockman, "A comparison of the full and half toroidal continuously variable transmissions in terms of dynamics of ratio variation and efficiency," *Mechanism and Machine Theory*, vol. 121, pp. 299–316, 2018.

[5] T. Capehart and C. A. Moore Jr, "Variable stiffness mechanisms using spherical continuously variable transmissions," in *ASME International Mechanical Engineering Congress and Exposition*, vol. 57397. American Society of Mechanical Engineers, 2015, Conference Proceedings, p. V04AT04A021.

[6] J. Zhang, J. Sheng, C. T. O'Neill, C. J. Walsh, R. J. Wood, J.-H. Ryu, J. P. Desai, and M. C. Yip, "Robotic artificial muscles: Current progress and future perspectives," *IEEE transactions on robotics*, vol. 35, no. 3, pp. 761–781, 2019.

[7] D. Bombara, R. Coulter, R. Konda, and J. Zhang, "A twisted string actuator-driven soft robotic manipulator," *IFAC-PapersOnLine*, vol. 54, no. 20, pp. 141–146, 2021.

[8] Y. J. Shin, K.-H. Rew, K.-S. Kim, and S. Kim, "Development of anthropomorphic robot hand with dual-mode twisting actuation and electromagnetic joint locking mechanism," in *2013 IEEE International Conference on Robotics and Automation*. IEEE, Conference Proceedings, pp. 2759–2764.

[9] S. H. Jeong, Y. J. Shin, and K.-S. Kim, "Design and analysis of the active dual-mode twisting actuation mechanism," *IEEE/ASME Transactions on Mechatronics*, vol. 22, no. 6, pp. 2790–2801, 2017.

[10] Z. Lu, R. Wang, Y. Xiao, T. Liu, C. Liu, and H. Zhao, "A load-adaptive hoisting mechanism based on spring-loaded rope and variable radius reel," *Advanced Robotics*, vol. 37, no. 23, pp. 1520–1531, 2023.

[11] S. Kim, J. Sim, and J. Park, "Elastomeric continuously variable transmission combined with twisted string actuator," *IEEE Robotics and Automation Letters*, vol. 5, no. 4, pp. 5477–5484, 2020.

[12] W. Shin, S. Park, G. Park, and J. Kim, "A passively adaptable toroidal continuously variable transmission combined with twisted string actuator," in *2022 International Conference on Robotics and Automation (ICRA)*. IEEE, Conference Proceedings, pp. 11 409–11 415.

[13] H. Singh, D. Popov, I. Gaponov, and J.-H. Ryu, "Twisted string-based passively variable transmission: Concept, model, and evaluation," *Mechanism and Machine Theory*, vol. 100, pp. 205–221, 2016.

[14] J. Jang, Y.-U. Song, and J.-H. Ryu, "Active-type continuously variable transmission system based on a twisted string actuator," *IEEE Robotics and Automation Letters*, vol. 7, no. 2, pp. 2605–2612, 2022.

[15] D. Popov, I. Gaponov, and J.-H. Ryu, "A study on twisted string actuation systems: Mathematical model and its experimental evaluation," in *2012 IEEE/RSJ International Conference on Intelligent Robots and Systems*. IEEE, Conference Proceedings, pp. 1245–1250.